Resonant optical scattering in nanoparticle-doped polymer photonic crystals

J. J. Baumberg,[1,][*] O. L. Pursiainen,[1] and P. Spahn[2]

[1]*NanoPhotonics Centre, Cavendish Laboratory, University of Cambridge, Cambridge CB3 0HE, United Kingdom*
[2]*Deutsches Kunststoff-Institut (DKI), Schlossgartenstrasse 6, D-64289 Darmstadt, Germany*

A broadband hyperspectral technique is used to measure the coherent optical backscatter across a wide spectral bandwidth, showing the resonant suppression of the photon transport mean free path around the photonic bandgap of a shear-assembled polymer photonic crystal. By doping with carbon nanoscale scatterers that reside at specific points within the photonic crystal lattice, the ratio between photon mean free path and optical penetration is tuned from 10 to 1, enhancing forward scatter at the expense of back-scatter. The back-scattering strength of different polarisations is not explained by any current theory.

Photonic crystals (PCs) have become of great interest for both science and technology because they promise new ways to control the flow of the light using structure on the subwavelength scale. Applications include enhanced light extraction from LEDs,[1] ultrahigh-Q low-volume microcavities,[2] dense optical integration and sensing,[3] while new physics is seen in enhanced emission rates,[4] photon localization and slow light.[5,6] While many applications concentrate on two-dimensional (2D) wave-guide photonic crystals because of their compatible microfabrication with current optoelectronics, three-dimensional (3D) photonic crystals promise enhanced properties such as nonlinear optical switching and trapping light.[7] A large amount of research thus aims to fabricate 3D photonic crystals with the highest possible dielectric contrast, Δn, to modify the transmission or reflection of light. However the physics of low-refractive index contrast 3D photonic crystals introduces new effects leading to enhanced tuneable structural color which are poorly understood. Indeed structural color in nature is more dependent on angular scattering than on specular reflectivity (which requires precise alignment of bionanostructure, sun, and viewer).

Here we show that recently-developed polymeric PCs based on large-scale shear-assembly of core-shell spheres demonstrate unusual resonant scattering properties. While PCs normally produce resonant *reflection* stopbands at the photonic bandgaps, here it is the angular scattering phenomena which are enhanced. Despite their low dielectric contrast, these nanomaterials display striking scattering-based structural color,[8] with sharp transmission edges.[9] To study the photon mean free path in detail, we adapt the coherent back-scattering (CBS) technique using white light lasers, and show how photon transport depends not just on particular configurations of scatterers, but also on the optical wavelength in such ordered photonic environments.

Polymer PC samples are fabricated using a scalable method, described in more detail in Refs. 8 and 10, which can produce tens of meters of single-domain mm-thick films of *fcc*-ordered PC. Cross-linked polystyrene spherical cores are chemically coated with polyethylacrylate (PEA) shells such that, under moderate temperature and pressure, shear-forces self-assemble the spheres into regular fcc packing [Fig. 1(a)].[11] Both compression and extrusion generate highly ordered PC layers through a process which is under

active investigation,[12] with the (111) layers parallel to the flat surfaces. Using core-shell spheres of 200–300 nm diameter results in photonic bandgaps completely tuneable across the visible spectrum. Tuning can also be achieved by stretching or compressing elastomeric samples,[9] and by angle tuning [Fig. 1(b)].

A critical additional design parameter is the ease of incorporating sub-50-nm-diameter nanoparticles into the photonic lattice, by premixing them with the core-shell particles. Because they sit within the soft outer PEA coat, they are embedded only at the interstices of the sphere array, providing a straightforward method to realize complex photonic structures. Here we use sub-0.1% by weight loadings of carbon nanoparticles of typical 20–30 nm compact size [Fig. 1(a)]. Electron microscopy (TEM) shows that the addition of this density of nanoparticles does not disrupt the uniformity of the fcc packing, but has a drastic effect on the apparent color of the samples [Fig. 1(c)]. Without the carbon, samples appear white (similar to artificial opals) unless held at a specific Bragg angle to the illumination source when they aquire a
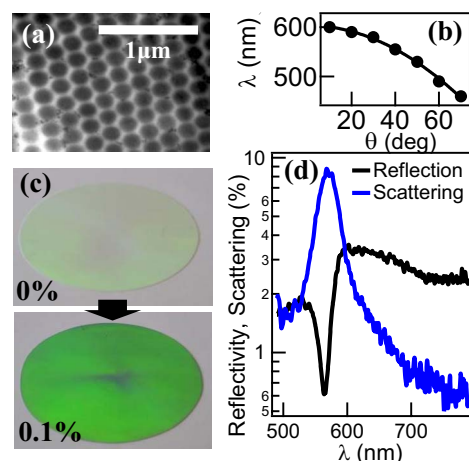
FIG. 1. (Color online) (a) TEM cross section of polymer photonic crystal stained to bring out carbon nanoparticles, loaded to 0.2%. (b) Angular tuning of (111) Bragg resonance matches expected theory (line). (c) Optical images of 20cm-wide compressed opal sheets both without and with 0.1% carbon nanoparticle loading. (d) Specular reflection and forward scattering spectra at 30° incidence.
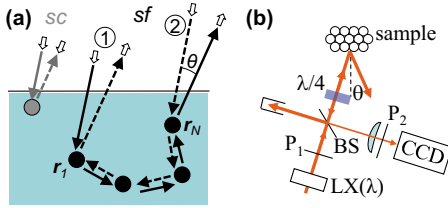
FIG. 2. (Color online) (a) Coherent backscatter showing interference between paths 1 and 2. Spin-conserving (*sc*) and spin-flipped (*sf*) cases refer to photon spin (open arrows). (b) Schematic CBS technique: selected collimated colors incident on sample at θ through polarisers (*P*) and 50% beamsplitter (BS), with backscattered light focused onto CCD.

FIG. 3. (Color online) (a) Cross sections of CBS cone analyzed for different carbon nanoparticle loadings. Inset: CCD image of CBS cone imposed on quasi-isotropic background scatter. (b) and (c) Photon transport mean free paths in (b) *sf* and (c) *sc* channels at different wavelengths for increasing nanoparticle loading, with photonic bandgap for 30° (green, at 570nm) and 0° (gray, at 600nm) incidence shaded. In each case data with opposite polarisations P_1, P_2 is also shown.

colored tinge. When the carbon is added, the color becomes intense and is present at all angles to the illumination.

Using angle-resolved broadband spectroscopy on a range of such samples this color has been shown to arise from resonant scattering by the carbon nanoparticles within the PC lattice.[8] In contrast to typical high-Δn PCs, here reflectivity is *minimum* on the Bragg condition, while forward scattering is resonantly *enhanced* within a cone of $\pm 20°$ around the specular reflection [Fig. 1(d)]. Crucial to understand scattering is the mean free transport path of photons within the PC, measured here using the standard techniques of CBS initially with a narrow linewidth cw laser at $\lambda = 514$ nm. Light scattered around a loop path within the sample that emerges back into the original direction has two counter-propagating directions of travel of identical length [Figs. 2(a): 1,2], giving rise to constructive interference. This constructive interference has an angular width which depends on the distance between the first and last scattering events in the sample, and hence on the photon scattering mean-free path, l_W, roughly as[13]

$$\Delta \theta_{CBS} \simeq \frac{0.7}{2\pi} \frac{\lambda}{l_W}. \qquad (1)$$

The precise shape of this backscatter cone (used for the fits here) has been shown to depend on many factors such as the material surface reflectivity, absorption, finite sample size and anisotropy.[14]

Here we develop the capability for exploring photon transport at different wavelengths in order to explore the effect of the periodic environment on scattering. The CBS setup [Fig. 2(b)] is based on a conventional polarization-resolved configuration but amended to allow illumination from the filtered output of a white light fiber laser (Fianium).[15] We use achromatic collimation optics and select 5 nm spectral slices from 450–800 nm using a liquid-crystal variable retarder. The CBS technique depends on collimated illumination of a sample at a specific angle, and measurement of the enhanced cone which is retroreflected exactly into the incident direction. To avoid speckle, the sample is spun about its normal at 50 Hz. Achromatic high-extinction polarisers are used to select incident (P_1) and backscattered (P_2) polarisations, and an ultra-broadband quarter wavelength plate is used to convert these to circular polarisations at the sample. Singly scattered light (e.g., from surface im-

perfections) converts right-circular to left-circular polarisations, and hence vertical-linear to horizontal linear at the detector (spin-conserving channel denoted *sc*). This single-scatter component is absent in the orthogonal spin-flipping (*sf*) channel which is thus used to extract l_W. Using an achromatic lens, different emission directions are converted into position on a charge-coupled device (CCD) with angular resolution of 0.05 mrad.

The setup is calibrated using CBS signals from diffusers and colloidal sphere suspensions, and found to match previous data on nonresonant samples. The azimuthally-symmetric backscatter cones [Fig. 3(a)] at each wavelength and polarization are appropriately normalized to compensate for incident intensity and the optics. Polarization-dependence of the beamsplitter is carefully removed in this process. For the data shown here we use an incident angle of 30° on a sample built from spheres $D = 235$ nm, with a refractive index core-shell contrast $\Delta n = 0.11$, which has the main (111) Bragg resonance at $\lambda_B = 570$ nm. We find good agreement with previous data taken using a 514 nm Ar laser.[8] As expected, introduction of the carbon nanoparticles decreases the photon mean free path leading to a broadening of the CBS multiple-scattering (*sf*) peak [Figs. 3(a) and 3(b)]. Without carbon, at longer wavelengths where the light averages over the internal structure of the photonic lattice, the mean free path approaches 120 μm exceeding 500 lattice planes between scattering events. Previous work on sedimented opals suggests that point defects (by sphere vacancies) dominate scattering,[16] and our microscopy reveals these to be low density in our opals. Adding only 0.1% carbon shortens the mean free path by an order of magnitude, much shorter than the measured absorption length which exceeds 100 μm.[8] The effect of absorption is however noticeable in the rounding of the CBS peak cusp, which arises from the selective pruning by absorption of long photon paths (which provide the interference at small cone angles).

Measurements taken in the orthogonal (*sc*) polarization, in which CBS is *completely absent* for diffusers or colloid suspensions, here show a *significant peak* which is broader than the *sf* channel [Fig. 3(c)]. The only photons that can contribute to this peak must have scattered more than once (to be able to give loop paths that can interfere) and also have their polarization rotated inside the sample. The effective mean free path for this polarization is >5 times shorter than for the multiple-scattered *sf* channel. Such anisotropic response has only recently been observed but for cold atoms[17] where polarization rotation arises from spin-selection rules of the resonant atomic transitions. For PCs polarization rotation can arise from either diffuse transport through anisotropic photonic crystal bands, or from high-angle scattering. The latter is more sensitive to polarization rotation from nonspherical defects (see below) and also causes photons to exit the sample at a shallower depth, producing shorter effective mean free paths, as observed.

Previous measurements on sedimented opals using fixed laser wavelengths or angle-tuning have found enhanced CBS cone widths on the Bragg resonance.[18,19] Here we resolve the full spectral dispersion of the CBS signal at fixed θ. While a threefold decrease in l_W is seen tuning from $\lambda \gg \lambda_B$ to $\lambda = \lambda_B$, a resonant dip in l_W is observed more clearly in the *sc* polarization channel. Most surprising is the observation that at shorter wavelengths when the optical field is most concentrated in the low refractive index shell matrix that holds the carbon nanoparticles, a *weaker* reduction in l_W with doping is observed.

Following Refs. 18 and 20, CBS is seen to arise from an average over all possible depths of first and last scatterers with a kernel $[1+\cos(k_{in}+k_{out})\cdot(r_1-r_N)]P(z_1)\Pi(z_1,z_N)P(z_N)$ inside this integral. Here the probablity that a photon reaches depth, z_i, is given by $P(z_i)=(1/l^*_{eff})\exp(-z_i/l^*_{eff})$, and Π is a diffusive transfer probability between first and last scatterers. Previous discussions have suggested that Π should be independent of PC structuring,[21] while the influence of the PC is mainly to reduce the penetration depth, L_B, of photons thus restricting scattering to shallower depths so that $(l^*_{eff})^{-1}=(l^*_z)^{-1}+[L_B(\lambda)]^{-1}$. A reduction in the photon mean free path at the Bragg resonance is thus predicted when $l^*>L_B$ but has so far been observed only in the regime $l^*\sim L_B$ where it is weak.[18,20] In the polymer PCs, $\frac{l^*}{L_B}\simeq\frac{100\ \mu m}{9\ \mu m}>10$, however the expected strong dip in l_W at λ_B is much smaller than this expected 10-fold reduction. The other effect that influences l_W is the surface reflectivity since photons that are reflected back into the sample after back-scattering travel further, giving longer effective l_W. This effect (which dominates in Ref. 20) should be reversed in our samples since the reflectivity shows a dip, not a peak, on the Bragg resonance [Fig. 1(d)].

One possible explanation for this discrepancy with theory can be that the group velocity dispersion near band-edges in specific directions influences the angularly averaged photon diffusion in Π.[22] Another effect not previously considered in PCs is the change in the scattering cross section as the wavelength tunes across the Bragg resonance, due to the different field distibution within the core/shell lattice. On the long λ side, the light is concentrated inside the spheres, while on the short λ side, the light is in the PEA,[9] and thus more sensitive
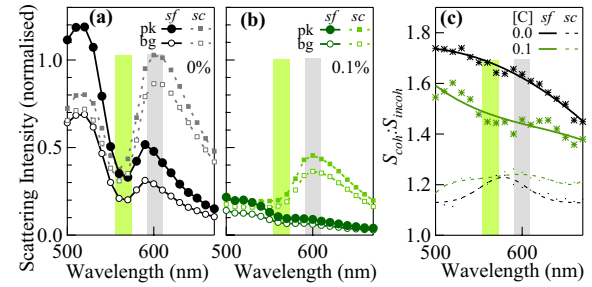
FIG. 4. (Color online) Coherent (CBS, ●) and incoherent (background, ○) backscatter intensities for (a) undoped and (b) 0.1% carbon doped polymer PCs. (c) Ratio of coherent (peak) to incoherent (background) scattering.

to the doped scatterers as well as lattice disorder. Hence $l^*_z=\Sigma p(z_i)z_i$ where $p(z_i)$ is the probability of a scattering event at depth z_i, should be controlled by the changing scattering cross section with λ, contributing to the spectral dependence seen in Fig. 3(b). However this cannot fully account for our results since approaching the bandgap from long wavelengths first reduces the field overlap with the scatterers, which should lead to an increase in l^* that is not observed.

When carbon nanoparticles are added, the CBS becomes much weaker [leading to the greater noise in Fig. 3(b)]. The strength of the coherent backscatter scattering peaks and the scattering background (normalized to the Lambertian background scatter from a diffuser plate) is shown in Fig. 4 as a function of wavelength. In all cases for the usual *sf* channel we observe that both the CBS peak and the background (incoherent contribution) are enhanced to shorter wavelengths, with a pronounced dip observed at the Bragg wavelength for the particular angle of incidence used. This >3-fold suppression of back-scattering when the light builds up standing waves inside the photonic crystal is similar to the observed dips in l_W [Fig. 3(b)] and not predicted by current models. However it is consistent with the observation that forward scatter is *resonantly enhanced* in precisely this condition, with incident light almost entirely redirected into a forward scattering cone around the specular direction of width $\pm 20°$.[8] It also contrasts with previous transmission measurements[9] which show strong absorption at all wavelengths shorter than the bandgap.

The ratio between CBS peak and background (which should be exactly 2 for the interfering counter-propagating paths without absorption) drops from 1.76 at 500 nm to 1.45 at 700 nm, unaffected by the Bragg resonance [Fig. 4(c)]. Previous attributions of this reduced ratio have been due to absorption, imperfect illumination, and reduced angular resolution, however the latter two explanations are discounted by our observations of colloidal sphere samples, and absorption should actually decrease to longer wavelengths. As the carbon loading is increased [Fig. 4(b)], the strength of all the scattering peaks decreases due to the additional absorption (particularly for $\lambda < \lambda_B$), however the CBS to background ratio is only slight reduced. Since this ratio should be equally affected by the absorption, it suggests long photon scattering paths (which give rise to the angular peak) are somehow pruned, even in the undoped polymer PCs.

Also unexpected is the strength of scattering in the *sc* channel (that includes single scattering events only in the background component) which for $\lambda > \lambda_B$ dominates the scattering. This switching from spin-flipped scattering to spin-conserved scattering as the wavelength is scanned across the photonic bandgap is also observed for increased carbon nanoparticle loading. The maximum *sc* scattering is observed at wavelengths around the normal-incidence bandgap at 601nm, where the optical field is predominantly inside the high refractive index spheres, suggesting spheres shifted sideways in each close-packed layer (producing an anisotropy) may be responsible for these strong polarization-flipping high angle events. While the low-angle *sf* channel decreases by a factor of 6 on 0.1% carbon doping (similar to the decrease in l_W), high-angle *sc* scattering is only halved emphasizing that at long-λ the field distribution is inside the spheres, away from absorption centers.

These results show a complex interplay between absorption and scattering in ordered 3D photonic environments. The introduction of nanoparticles at localized points within the lattice introduces a strong sensitivity of the scattered light to wavelength and angle. Using a broadband spectroscopic coherent backscatter technique enables measurement of the photon mean free path and scattering strength for wavelengths above and below the photonic bandgaps. While the photon mean free path is reduced at the photonic bandgap by adding carbon nanoparticles, both coherent and incoherent scattering are also resonantly suppressed. The resonant reduction of light penetration at the Bragg resonance resonantly modifies the longer photon mean free paths. The appearance of spectrally-resonant polarization-flipped scattering suggests at least two origins for scattering in these samples. These observations should stimulate the development of models for scattering in periodic environments which do not yet exist, and are important for the understanding and development of structural color and sensor applications.

*jjb12@cam.ac.uk

[1] Alexei A. Erchak, Daniel J. Ripin, Shanhui Fan, Peter Rakich, John D. Joannopoulos, Erich P. Ippen, Gale S. Petrich, and Leslie A. Kolodziejski, Appl. Phys. Lett. **78**, 563 (2001).

[2] Y. Akahane, T. Asano, B.-S. Song, and S. Noda, Nature (London) **425**, 944 (2003).

[3] M. Lončar, A. Scherer, and Y. Qiu, Appl. Phys. Lett. **82**, 4648 (2003).

[4] E. Burstein and C. Weisbuch, *Confined Electrons and Photons: New Physics and Applications* (Plenium, New York, 1994).

[5] F. Xia, L. Sekaric, and Y. Vlasov, Nat. Photonics **1**, 65 (2007).

[6] H. Y. Ryu and M. Notomi, Opt. Lett. **28**, 2390 (2003).

[7] S. John, Phys. Rev. Lett. **58**, 2486 (1987).

[8] O. L. J. Pursiainen, J. J. Baumberg, H. Winkler, B. Viel, and T. Ruhl, Opt. Express **15**, 9553 (2007).

[9] O. L. J. Pursiainen, J. J. Baumberg, K. Ryan, H. Winkler, B. Viel, and T. Ruhl, Appl. Phys. Lett. **87**, 101902 (2005).

[10] T. Ruhl, P. Spahn, and G. P. Hellmann, Polymer **44**, 7625 (2003).

[11] O. L. J. Pursiainen, J. J. Baumberg, H. Winkler, B. Viel, P. Spahn, and T. Ruhl, Adv. Mater. **20**, 1484 (2008).

[12] D. S. Snoswell, A. Kontogeorgos, J. J. Baumberg, T. D. Lord, M. R. Mackley, P. Spahn, and G. P. Hellmann, Nano Lett. (to be published).

[13] R. Corey, M. Kissner, and P. Saulnier, Am. J. Phys. **63**, 560 (1995).

[14] M. B. van der Mark, M. P. van Albada, and A. Lagendijk, Phys. Rev. B **37**, 3575 (1988).

[15] O. L. Muskens and A. Lagendijk, Opt. Express **16**, 1222 (2008).

[16] R. Rengarajan, D. Mittleman, C. Rich, and V. Colvin, Phys. Rev. E **71**, 016615 (2005).

[17] G. Labeyrie, C. A. Mueller, D. S. Wiersma, C. Miniatura, and R. Kaiser, J. Opt. B: Quantum Semiclassical Opt. **2**, 672 (2000).

[18] J. Huang, N. Eradat, M. E. Raikh, Z. V. Vardeny, A. A. Zakhidov, and R. H. Baughman, Phys. Rev. Lett. **86**, 4815 (2001).

[19] A. F. Koenderink, M. Megens, G. van Soest, W. L. Vos, and A. Lagendijk, Phys. Lett. A **268**, 104 (2000).

[20] E. Akkermans, P. E. Wolf, and R. Maynard, Phys. Rev. Lett. **56**, 1471 (1986).

[21] Band gaps restrict photon transport only for very small angular zones of the 4π steradian diffusive scattering cone.

[22] M. V. Erementchouk, L. I. Deych, H. Noh, H. Cao, and A. A. Lisyansky, J. Phys.: Condens. Matter **21**, 175401 (2009).